Toward multicomponent bioluminescence imaging via statistical modeling and tuning emission wavelength.

by Suong B. A. Tran

Submitted in partial fulfillment of the Honors Requirements for the Chemistry Department
Dickinson College

Professor Colin Rathbun, Research Supervisor
Professor Micheal Holden, Academic Supervisor
Professor Jim Rego, Reader
Professor Connor Rebecca, Reader
Professor Sarah St. Angelo, Reader

Carlisle, Pennsylvania
May 2023

Contents

List of Figures

Acknowledgements

I would like to express my deepest gratitude to Professor Colin Rathbun, my research supervisor, for his support and guidance throughout my honors thesis. His dedicated involvement in every step of the process has been invaluable, and I would like to express my sincere appreciation for his assistance and understanding over the past years.

I would also like to thank the professors and faculty members in the Chemistry department for their encouragement and contributions to my academic journey. Their commitment to teaching and mentorship has been a constant source of inspiration and motivation. I also want to express my gratitude to Professor Eren Bilen from Data Analytics Department for assisting me with developing statistical model, Donald Carr for arranging all the necessary chemicals for my experiments, and to Daniel Hockersmith for ensuring that all the instruments were running smoothly.

I am also grateful to the members of my research group and laboratory colleagues for their encouragement and support. In particular, I would like to thank Abigail McGahan and Roberta Akrong for their assistance in providing me with the data needed for my research.

Moreover, I would like to acknowledge Dickinson Research and Development for sponsoring the research. Their support has been critical in allowing me to complete my honors thesis.

Suong B. A. Tran

Introduction

Bioluminescent imaging has been developed over the last decade as a tool for studying and analyzing biological functions, which demands probes that can report on processes over time within living organisms. It offers sensitive imaging in cells and tissues without the need for surgery.[1] With bioluminescent tools, researchers can "see" biological processes in real-time, providing critical insights into the functions of living organisms. Bioluminescence occurs when a luciferase enzyme catalyzes the oxidation of its luciferin substrate, resulting in the visible production of light (Figure 1A).[2] Unlike other imaging techniques, such as fluorescence imaging, bioluminescence offers various advantages, including lower background signal and no need for excitation light.[3] Bioluminescence imaging is a highly versatile technology that has gained popularity in cancer research and studying complex interactions (e.g. host-pathogen) *in vivo*.[4] It can also be employed in numerous applications, such as investigating protein-protein and protein-ligand interactions, exploring gene regulation, and studying cell signaling.[5, 6]

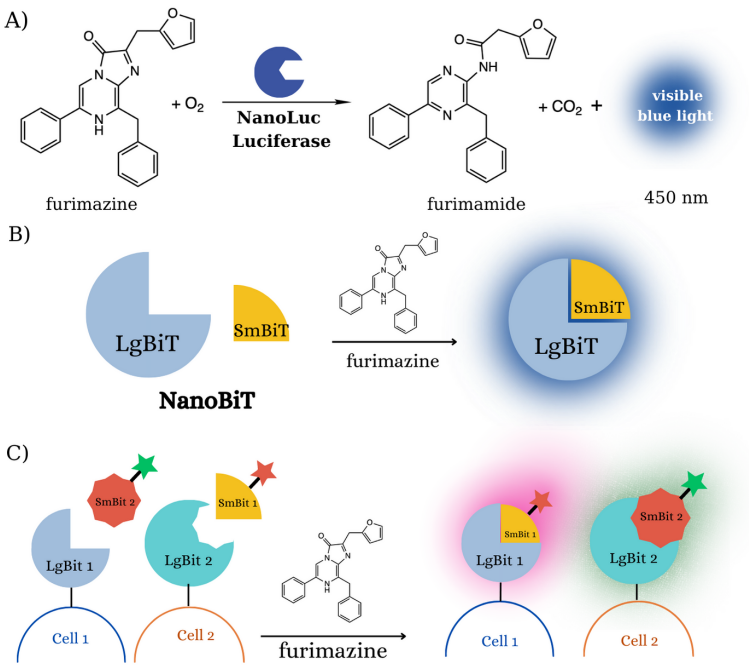

Figure 1: (A) Luciferase reaction of NanoLuc in the presence of furimazine. (B) The association of SmBiT and LgBiT in the presence of furimazine generates blue light. (C) Multi-component imaging of two different cell types with engineered NanoBiT enzymes will require the SmBiT-LgBiT binding interaction and tuning emission wavelength with fluorophores.

The major limitation of bioluminescence imaging *in vivo* is that it can only image one population of cells at a time. The development of a multicomponent bioluminescence imaging tool would enable researchers to study complex interactions in tandem. With at least

two new colors, the bioluminescent tools could be developed to enable visualizing multiple cell types in mouse models (Figure 1C). Because of their utility, enhanced bioluminescence imaging techniques are needed to allow researchers to "see" new biological processes.

To develop enhanced bioluminescent tools, it is important to start with a bright and robust luciferase enzyme. We chose NanoLuc, the newest commercially available luciferase enzyme, derived from the deep-sea shrimp *Oplophorus gracilirostris*. It emits glow-type luminescence 150-fold greater than firefly-based enzymes.[7] Particularly, we are interested in NanoBiT, a split reporter system based on the luciferase enzyme NanoLuc. NanoBiT is composed of two subunits: a small peptide consisting of 11-13 amino acids (SmBiT) and a larger 18 kDa enzyme (LgBiT). Similiar to NanoLuc, the association of SmBiT and LgBiT gives bioluminescence with blue light in the presence of furimazine – the luciferase substrate (Figure 1B).[8] NanoBiT was chosen for our research because of the ease in modulating the bioluminescence properties only by modifying its subunit - SmBiT, instead of dealing with the entire luciferase enzyme.

In addition to the development of multicomponent bioluminescence imaging techniques, it is significant to note another drawback of NanoBiT that its emitted light is blue (450 nm). Within the visible spectrum, hemoglobin is the primary chromophore in blood cell that absorbs light. Hemoglobin absorbs primarily in the blue and green part of the visible spectrum.[9] This phenomenon can be attributed to short-wavelength light, such as blue light, is less permeable through tissues than longer-wavelength light.[9, 10] Therefore, to enable the visualization of cell populations in live mice, it is necessary to red-shift the color of light emission of NanoBiT probes. To modulate the light emission color of NanoBiT, we

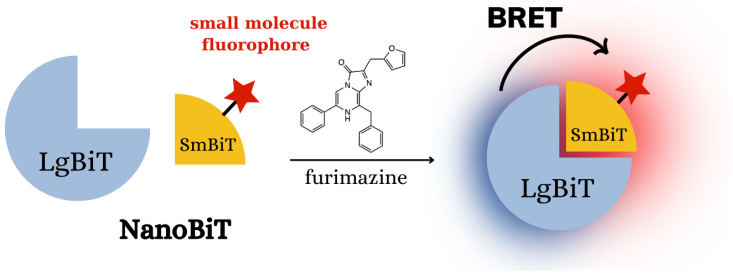

Figure 2: SmBiT and LgBiT bind together in the presence of furimazine, and blue light is emitted. Resonance nergy is transferred to the fluorophore which then emits a longer wavelength of light.

will take advantage of bioluminescence resonance energy transfer (BRET). BRET is the process of dipole-dipole non-radiative energy transfer from a luciferase energy donor to an acceptor fluorophore.[11] Previous work concatenated NanoLuc with fluorescent proteins to red-shift emission via BRET.[12] Another study showed that the color of NanoLuc is also tunable via BRET with small-molecule fluorophores via HaloTag and SNAP-tag probes.[13] However, these techniques require bulky proteins, and do not enable true multi-component imaging. Based on the principle of BRET, we have developed an easier technique to tune the color of bioluminescence by taking advantage of BRET and NanoBiT. We modulated the emission wavelength of NanoBiT by chemically appending a fluorophore to the N-terminus of SmBiT peptide (Figure 2). In the presence of furimazine, the association of SmBiT and LgBiT enabled BRET, shifting the emitted blue light to near-red light. With this technique, I successfully modulated the color of NanoBiT from blue to three new colors (cyan, green, and yellow).

To enable the use of these probes in multicomponent imaging, our laboratory has introduced mutations to the amino acids at the binding pocket of LgBiT to selectively bind each SmBiT. We utilized deep mutational scanning to analyze the frequency of each mutation appeared before and after binding to two different SmBiTs.[14] We developed generalized linear model (GLM), a statistical model, to predict the contribution of binding preference between two SmBiTs. Predicted mutations preferring specific SmBiTs are also known as "hits". Investigating the light emission of significant "hits" predicted by the model with the equal combination of two SmBiTs showed that even single mutations of LgBiT can result in distinction of binding preference between SmBiTs.***This study has demonstrated that we are able to red-shift the emitted light of NanoBiT and develop an easy-to-use technique for multicomponent bioluminescence imaging.***

Materials and Methods

General Information

Chemicals and Supplies. All commercial reagents were used as received without purification. An anhydrous and amine-free form of N,N-dimethylformamide (DMF) was obtained from Sigma-Aldrich. Acetonitrile and deionized water used for liquid chromatography, each containing 0.1% trifluoroacetic acid (TFA), were bought from Sigma-Aldrich (HPLC grade) for use in analytical and preparative reverse-phase HPLC. Rink amide resin, Fmoc-protected amino acids, and peptide coupling reagents, consisting of HCTU, HOAt (0.6 M in DMF), PyAOP and DIEA, were acquired from CHEM-IMPEX for peptide synthesis. 4-methylpiperidine was obtained from TCI.

Instrumentation. Analytical reverse-phase LCMS involved an Agilent 6110 Quadrupole LC/MS and 1200 LC instrument, equipped with an Eclipse Plus C18 column (3.5 µm, 100 × 4.6 mm). A gradient of acetonitrile and water, each containing 0.1% TFA, was used to elute peptides from 5% to 100% over a period of 30 minutes. Peptides were purified using a Waters preparative reverse-phase HPLC system, which included a Waters 2489 UV-Vis detector, a Waters 1525 Binary HPLC Pump, and a Waters fraction collector III. Bioluminescence imaging was performed on a Synergy H1 microplate reader from BioTek.

Synthesis of SmBiT peptide

SmBiT peptides were synthesized on Rink amide resin using solid-phase peptide synthesis. Rink Amide resin (54.9 mg, 0.91 meq/g) was added to 5 mL solid-phase peptide synthesis PPE vessel. The resin was then swollen with 4 mL of DMF for 1 hour. The coupling cycle consisted of Fmoc-deprotection with of 20% v/v 4-methylpiperidine in DMF (3 mL) for 20 min at room temperature, coupling of the amino acid (0.15 mmol, 3 equiv) with HCTU (0.15 mmol, 3 equiv) and DIEA (0.45 mmol, 9 equiv) in dry DMF (3 mL) for 1

hour. After each reaction, the resin was washed with dry DMF (3 x 3 mL).

Synthesis of SmBiT-fluorophore conjugates

The following quantities of reagents was used when coupling fluorophore fluorescein (FAM). FAM (12 mg, 5 equiv) was appended to the SmBiT on resin (18 mg) on resin using HOAt (53 µL, 5 equiv), PyAOP (15 mg, 5 equiv), and DIPEA (11uL, 10 equiv), following by washing the resin with dry DMF (3 x 3 mL). The peptide-fluorophore was then cleaved from the resin using the solution of phenol (5%w/w), water (5%v/v), triisopropylsilane (5%v/v), thioanisole (5%v/v), ethandithiol (2.5%v/v), and trifluoroacetic acid (82.5%v/v). The sample obtained after cleavage was precipitated in cold diethyl ether, followed by centrifuging and washing with diethyl ether. Subsequently, the resulting precipitate was subjected to preparative high-pressure liquid chromatography (prep-HPLC) to separate the fluorophore-peptide and uncoupled peptide components. The isolated solid fluorophore-peptide was then obtained through lyophilization. The verification of purity and mass of the SmBiT-fluorophore conjugates was accomplished by utilizing liquid chromatography-mass spectroscopy (LCMS) (Figure S2-5).

Bioluminescence Imaging

Emission Spectrum

The BRET efficiency of the new conjugates with native LgBiT was measured based on the emission spectrum of NanoBiT. LgBiT was expressed in *E. coli* by autoinduction in shaking cultures for 24 hours. Cells were lysed with lysis buffer (50 mM Tris HCl, 500 mM NaCl, 0.5% (v/v) Tween, 5 mM $MgCl_2$, pH = 7.4). PBS was added to lyophilized SmBiT-fluorophore conjugates and the concentration was determined using UV-Vis with molar absorption coefficient of the fluorophore. 50 µL of LgBiT was combined with 50 µL of SmBiT-fluorophore conjugates at the final concentration of 100 nM in a 96-well plate. The

emission spectra were taken in 5-nm steps on the Synergy H1 plate reader in the presence of 5 µL of 1:50 diluted furimazine (Nano-Glo, Promega). The amount of bioluminescence is measured in relative light units (RLU), and averages were calculated from three replicates at each wavelength. The original SmBiT was used as the positive control for the experiment to assure that the association of SmBiT and LgBiT gives blue light (λ_{em} = 450 nm).

Because BRET is not 100% efficient, there was small peak of blue light (450 nm). Observed BRET efficiency was determined by the ratio of light emission at 450 nm and maximum wavelength of the new color:

$$\text{Observed BRET efficency} = \frac{\mathrm{I}_{\lambda_{\text{new color}}}}{\mathrm{I}_{450\mathrm{nm}} + \mathrm{I}_{\lambda_{\text{new color}}}}$$

Permeability through mimic tissue

The same experiment of bioluminescence imaging as described above was executed; however, the 96-well plate was now imaged in the absence and presence of mimic tissue (1 mm thickness, ham) covering the well. Tissue permeability (transmitted percentage) was calculated by:

$$\%\ \text{transmitted} = \frac{\mathrm{I}_{\text{with mimic tissue}}}{\mathrm{I}_{\text{with out mimic tissue}}}$$

Statistical model to predict selective-binding mutations of LgBiT

To utilize these NanoBiT-fluorophore conjugates for multi-component imaging, a statistical model was developed to finding LgBiTs that selectively bind specific SmBiTs. SmBiT 1 (VSGWRLFKKIS) and SmBiT 2 (VEGYRLFEKIS) were screened separately against the library of LgBiT mutants and their sequences were determined by high throughput sequencing. Deep mutational scanning was used to analyzed the observed sequences, and how frequent each mutation appeared before (Count library) and after (Count SmBiT) binding to SmBiT.[14, 15] Generalized Linear Model (GLM) was adapted to better estimate the contribution of each mutation to the binding difference between SmBiT 1 and SmBiT

2 based on their sequence count, normalized to the count of wild type (WT).[16, 17] The difference in observed count after binding each SmBiT was calculated by:

$$\text{Difference} = \frac{\frac{\text{Count}_{\text{Mutation\_SmBiT2}}}{\text{Count}_{\text{WT\_SmBiT2}}} - \frac{\text{Count}_{\text{Mutation\_SmBiT1}}}{\text{Count}_{\text{WT\_SmBiT1}}}}{\frac{\text{Count}_{\text{Mutation}}}{\text{Count}_{\text{WT}}}}$$

$\text{Count}_{\text{Mutation\_SmBiT1}}$ and $\text{Count}_{\text{WT\_SmBiT1}}$ are, respectively, the observed counts of LgBiT mutant and WT when they were screened with SmBiT 1; similar to SmBiT 2. $\text{Count}_{\text{Mutation}}$ and Count_{WT} are, respectively, the observed counts of LgBiT mutant and WT when they were screened alone. GLM was applied on provided data using the following call in R.

All experiment data and coding scripts for GLM can be found on GitHub via the link (*https://github.com/tranJen/GLMNanoBiT_Honors_Thesis*). The README file will be helpful to navigate the data.

Testing "hits" from the developed model

Flourophore Cou343 (λ_{em} = 490 nm, cyan light) was appended on SmBiT 1 and fluorophore TAMRA (λ_{em} = 580 nm, yellow light) was appended on SmBiT 2. The similar experiment of bioluminescence imaging described above was executed. Instead of adding only one SmBiT to each well on 96-well plate, two SmBiT-flourophores were combined equally to each well with the total concentration of 100 nM, and a total volume of 50 µL.

Results and Discussion

Synthesis of SmBiT-fluorophore conjugates

We initially selected the fluorophore fluorescein (FAM) due to its affordable cost and longer-wavelength emission (λ_{em} = 520 nm, green light). Additionally, FAM has a carboxyl group that can be conveniently attached to the N-terminus of peptide, making it an attractive option for our purposes (Figure 3B). Previous research demonstrates that FAM can be attached to polyproline peptide (6-18 residues).[18] Polyproline peptides have a unique left-handed backbone with no hydrogen bond that differs from the α-helix or β-sheet structures commonly observed in normal proteins and peptides. Our objective was to investigate whether we could couple FAM to our SmBiT peptides.

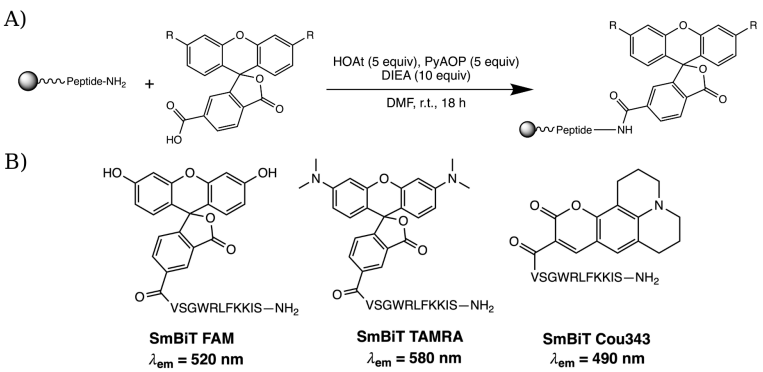

Figure 3: Structures of three targeted fluorophores that were appended to SmBiT. Each fluorophore exhibited a distinct emission wavelength.

After testing several conditions for peptide coupling, we were able to optimize the reaction conditions and develop the best method for synthesizing SmBiT-FAM conjugates using HOAt, PyAOP, and DIEA (Figure 3A). With the same conditions, two new fluorophores were appended to the same SmBiT: carboxytetramethylrhodamine (TAMRA), and Coumarin 343 (Cou343), which both have a carboxyl group (Figure 2B). Fluorophore Cou343 emits at 490 nm, corresponding to cyan light. Even though its permeability was expected to be not as good as SmBiT-FAM, it was synthesized with the ultimate goal of having different colors for multi-component imaging. Fluorophore TAMRA emits at 580 nm with yellow light. This fluorophore was expected to be preferable to FAM as near-red light is more tissue-permeable.

Emission Spectrum of NanoBiT-fluorophore conjugates

In the presence of furimazine, the interaction between SmBiT and LgBiT leads to bioluminescence emission of blue light. By introducing a fluorophore at the N-terminus of the SmBiT peptide, the bioluminescent energy emitted can be transferred to the fluorophore, resulting in the emission of longer wavelength light. If BRET was occurring, there would be a peak in the longer wavelength range corresponding to the emission of a new color, rather than the blue color peak at 450 nm.

The emission spectrum of luciferase reaction of SmBiT-fluorophore conjugate confirmed that BRET was occurring (Figure 4). The presence of a minor peak of blue light (450 nm) indicated that the BRET was not 100% efficient. Both NanoBiT-FAM (λ_{em} = 520 nm, green light) and NanoBiT-TAMRA (λ_{em} = 580 nm, yellow light) exhibited significant BRET, with observed BRET efficiencies of 85% and 91%, respectively. Although the observed BRET efficiency for NanoBiT-Cou343 (λ_{em} = 490 nm, cyan light) was slightly lower at 68%, this does not necessarily indicate poor performance in modulating the emission wavelength of NanoBiT. It is possible that the width of the cyan light peak from SmBiT-Cou343 may overlap with and contribute to the peak of blue light emission, potentially leading to a lower observed efficiency.

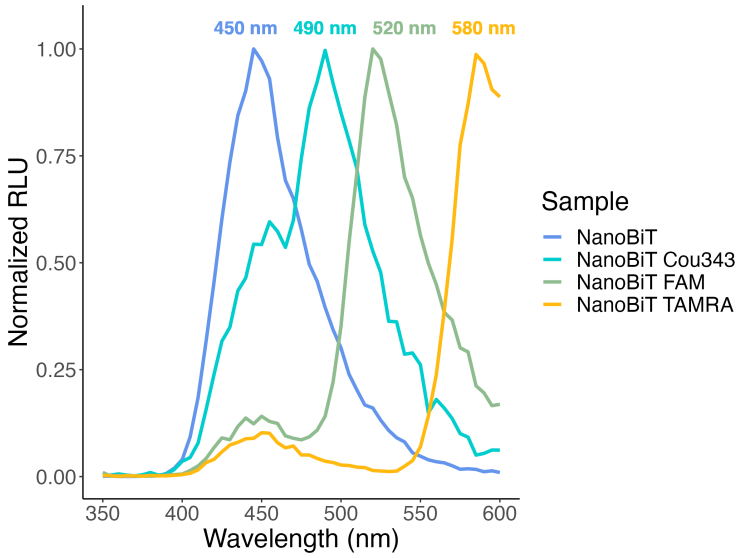

Figure 4: Emission spectrum of luciferase reaction of SmBiT, SmBiT-FAM, SmBiT-TAMRA.

Permeability through mimic tissue

After successfully generating new colors from the SmBiT-fluorophore conjugates, our next objective was to determine if light emission from these new conjugates was able to penetrate biological tissues sufficiently for utility in biological applications. Light emission was measured in the absence and present of mimic tissue, which is the slice of ham covering the well of a 96-well plate. Previous research used turkey bacon as mimic tissue for bioluminescence imaging.[19] We opted for ham over bacon because bacon can have uneven layers of fat and meat, a slice of ham provides a more consistent thickness and texture.

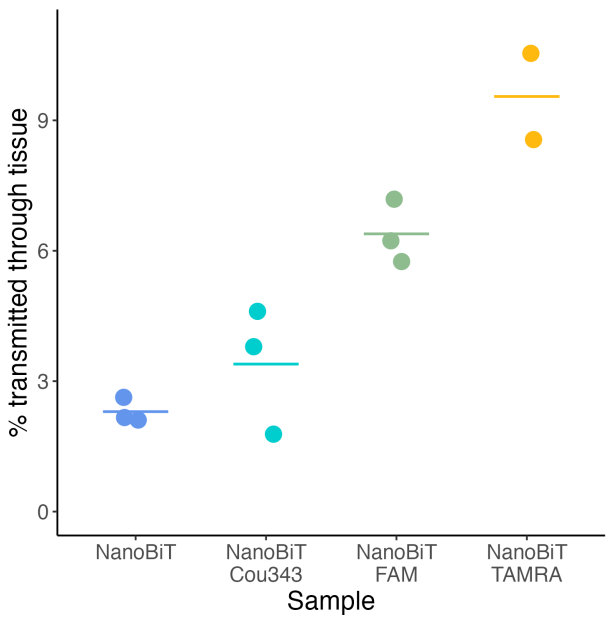

Figure 5: Comparison of permeability between navtive NanoBiT and three new NanoBiT-fluorophore conjugates. As expected, red-shift NanoBiT results in higher permeability (higher % transmitted through tissue).

The experiment supports the hypothesis that near-red light is more permeable in tissue (Figure 5). The calculated transmitted percentage of native NanoBiT is 2.6%. Transmitted percentage of NanoBiT-Cou343 and NanoBiT-FAM were improved to 3.8% and 5.7% respectively. NanoBiT-TAMRA also increased the transmitted percentage three times to 8.56%. These data indicated that the red-shifted light when using the SmBiT-fluorophore is more permeable than when using the original SmBiT. As part of future investigations, we intend to explore the use of other red fluorophores to further expand our understanding of this phenomenon.

In the absence of mimic tissue, the light emission of native NanoBiT was found to be higher than that of the NanoBiT-TAMRA because SmBiT-TAMRA has lower binding affinity than original SmBiT. However, when tested with mimic tissue, the light emission of the NanoBiT-TAMRA was slightly higher than that of native NanoBiT (Figure S1). We hypothesize that the reduced light emission observed with SmBiT-TAMRA, as compared to

native SmBiT in the absence of mimic tissue, is due to the steric hindrance resulting from the attachment of the fluorophore to the SmBiT. It might cause a poor fit at the binding interface, resulting in a lower binding affinity or higher dissociation constant (K_D). Less interaction between SmBiT and LgBiT can reduce light emission. To investigate this further, I plan to conduct experiments to determine the K_D for each SmBiT-fluorophore conjugate. To reduce steric hindrance and enhance bioluminescence, we plan to introduce a linker consisting of a few Glycine residues at the N-terminus of the peptide before attaching the fluorophore. The length of linker will be tested because long linker may result in lower BRET efficiency.

Single-mutation of LgBiT results in SmBiT binding difference

In order for these NanoBiT-fluorophore conjugates to be used in multi-component imaging, it is important to have LgBiTs that only bind certain SmBiTs. Our lab has been mutating amino acids at the binding pocket of LgBiT to have a selective binding for each SmBiT.

We have been investigating SmBiT 1 (VSGWRLFKKIS) and SmBiT 2 (VEGYRLFEKIS). SmBiT 1 (K_D = 700 pM) has a lower dissociation constant, indicating a higher binding affinity to native LgBiT compared to SmBiT 2 (K_D = 1.3 μM). This also implies that the association of SmBiT 1 and LgBiT generates a stronger light emission than that of SmBiT 2. Each of two other lab members, Abigail McGahan and Roberta Akrong, evaluated a library containing 736 LgBiT single-mutants at the binding pocket on the C-terminus. SmBiT 1 and SmBiT 2 were screened separately against the library of LgBiT mutants and their sequences were determined by high throughput sequencing. Deep mutational scanning was used to analyzed the observed sequences, and how frequent each mutation appeared before and after binding to each SmBiT.[14] We hypothesize that the difference in the number of mutants count for each SmBiT would significantly affect the selectivity for

each SmBiT.

After high throughput sequencing the library, the data set included 429 observations of LgBiT mutants. Generalized Linear Model (GLM) was applied to handle this large data set and predict the contribution of each mutation to the binding preference between SmBiT 1 and SmBiT 2.[16] GLM is a statistical framework for modeling relationships between explanatory variables and response variables. The modelling was developed in collaboration with Professor Eren Bilen from the Data Analytics Department. (My lab members are evaluating the single-mutants on the N-terminus, and multiple-mutants. Therefore, in the future, we intend to apply Random Forest regression to consider non-linear relationships as well.)

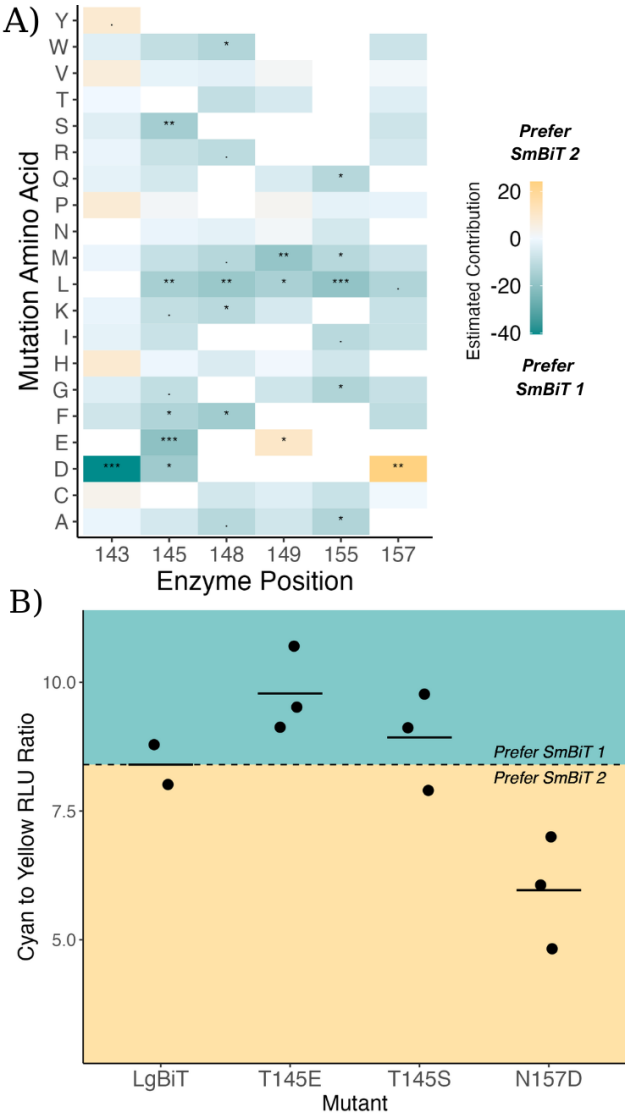

Figure 6: (A) Heat map of the contribution of each mutation at each position screened to the binding difference between SmBiT 1 (cyan) and and SmBiT 2 (yellow) predicted by generalized linear model (GLM). *Significant level code: 0 '***' 0.001 '**' 0.01 '*' 0.05 '.' 0.1 ' ' 1.* (B) Mutation N157D prefers binding SmBiT 2. Mutation T145E and T145S prefer binding SmBiT 1, and T145E causes a larger difference. The dashed line corresponds to the binding preference of wild type.

After running the analysis, the model predicted several mutations contributing to the binding difference between SmBiT 1 and and SmBiT 2 (Figure 6A). At the 0.01 level of significance, the mutants hypothesized to prefer binding SmBiT 1 (cyan block) were L143D, T145E, T145L, T145S, G148L, S149M, T155L. The mutant hypothesized to prefer binding SmBiT 2 (yellow block) was N157D.

Abigail McGahan and Professor Rathbun cloned several of these mutants of interest for further testing. Due to the unavailability of all mutations, only three mutants were used to test the prediction of the GLM, which were T145E, T145S, N157D. Even though mutant T145S was not predicted to as significantly contribute to binding difference between SmBiT 1 and SmBiT 2 as mutant T145E, this mutant was examined to see if the model correctly predicted the relative contribution to the difference. Mutant T145E was predicted to have larger contribution than mutant T145S.

To test if the GLM predicted correctly the contribution of each LgBiT mutation in binding difference between SmBiT 1 and SmBiT 2, a similar experiment of bioluminescence imaging described above was executed. Instead of adding only one SmBiT to the reaction, we equally added 25 µL of SmBiT 1 and SmBiT 2 and recorded spectra. Cyan to yellow luminescence ratio (the ratio of luminescence at 490 nm and at 580 nm), was used to analyze how the binding difference changed (Figure 6B).

Even though the result indicated that all three mutations (T145E, T145S, N157D) selectively bound to SmBiT 1 more than SmBiT 2 because the ratio is larger than 1, they did show difference relative to wild type (Figure 6B, dashed line) in the binding preference toward SmBiT. Mutants T145S and T145E were predicted to prefer binding SmBiT 1, and indeed, we were able to make the mutations to prefer the SmBiT 1 more than the wild type because their cyan to yellow ratios were higher than that of wild type. Furthermore, the model accurately predicted the relative impact of mutations on the binding difference between SmBiT 1 and SmBiT 2. As expected, mutant T145E resulted in a greater increase in the cyan to yellow RLU ratio than mutant T145S. Mutants N157D was expected to have a preference for SmBiT 2, but it was still preferred SmBiT 1. Even though this mutation did not completely switch preference to SmBiT 2, the experiment showed that the cyan to yellow RLU ratio was decreased below that of the wild type, indicating that it caused the LgBiT to prefer SmBiT 1 less. Noticeably, a single-mutation of LgBiT has already resulted in binding preference toward SmBiT 2. Introducing multiple mutation would would result in

a greater influence.

After observing that single mutations in the C-terminus of LgBiT can cause difference in the binding preferences between SmBiT 1 and SmBiT 2, we anticipate that combining multiple mutations could result in even larger differences. To validate the accuracy of the GLM predictions, we plan to test other significant mutants (Figure 6A). Additionally, future studies will also focus on exploring mutations at the N-terminus of LgBiT.

Conclusion

Three SmBiT-fluorophores with three new colors of cyan, green, and yellow light were synthesized and showed that the red-shifted light of NanoBiT via BRET is more permeable in tissue compared to orginal NanoBiT. In order for these NanoBiT conjugates to be further applied in cell visualisation in the bodies of live mice, we plan to label red fluorophore on SmBiT, such as Atto590 (λ_{em} = 622 nm).

Tested LgBiT mutants T145E, T145S, N157D behaved as predicted by GLM. To ensure the accuracy of the model's predictions for all mutants, further significant mutants will be tested in future studies. With the ultimate goal of developing multi-component imaging technique, a combination of predicted mutants will be studied in order to enhance the binding preference between SmBiT 1 and SmBiT 2. Furthermore, the binding selectivity between two SmBiTs can be improved by exploring mutations on the N-terminus of LgBiT.

We believe our findings hold great significance for advancing bioluminescence imaging. The development of small and easy-to-use red NanoLuc-based probes enables multicomponent imaging, which can facilitate the study of complex interactions in living organisms. Ultimately, this research may shed light on the study of interaction between cancer cells and the immune system *in vivo*.

Supplementary Information

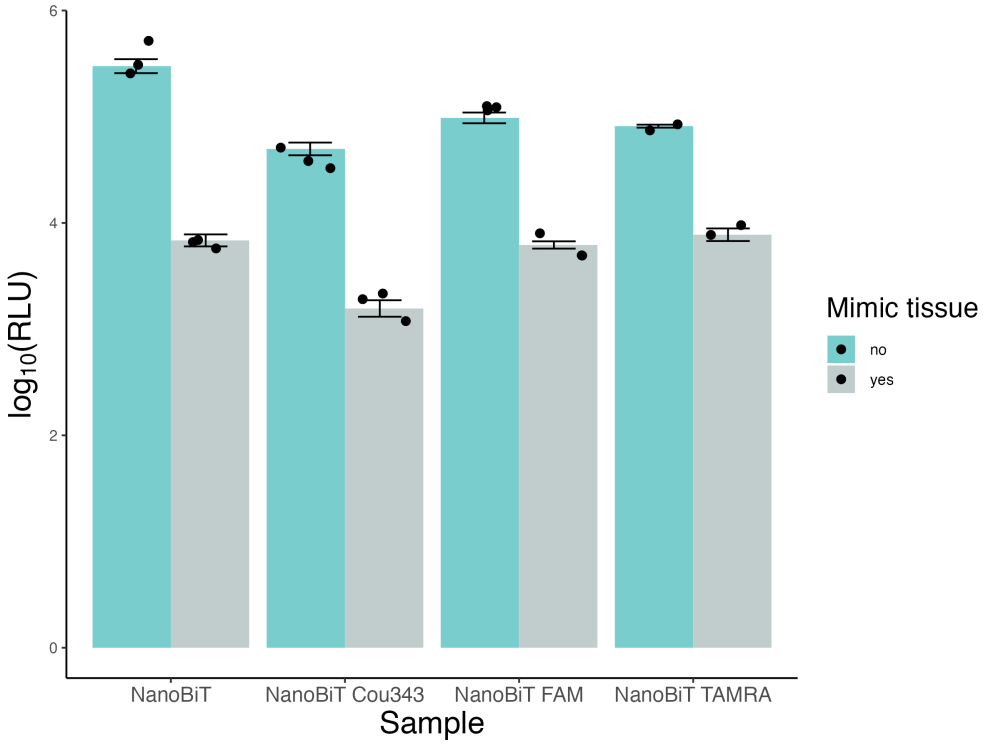

Figure S1: Light emission of native NanoBiT and NanoBiT-fluorophore conjugates in mimic tissue experiments show that light emission of native NanoBiT is heavily absorbed by the tissues compared to that of NanoBiT-TAMRA.

The synthesized SmBiT-fluorophore conjugates were characterzied by LC-MS.

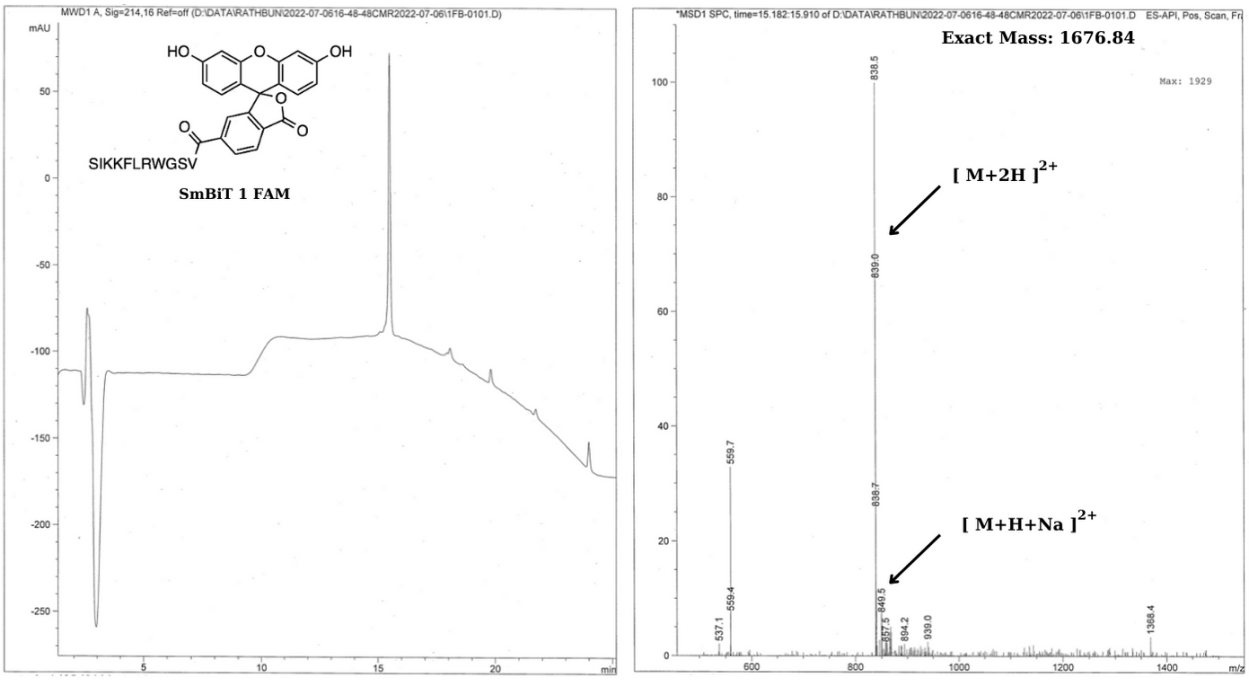

Figure S2: Characterization of SmBiT 1 - FAM

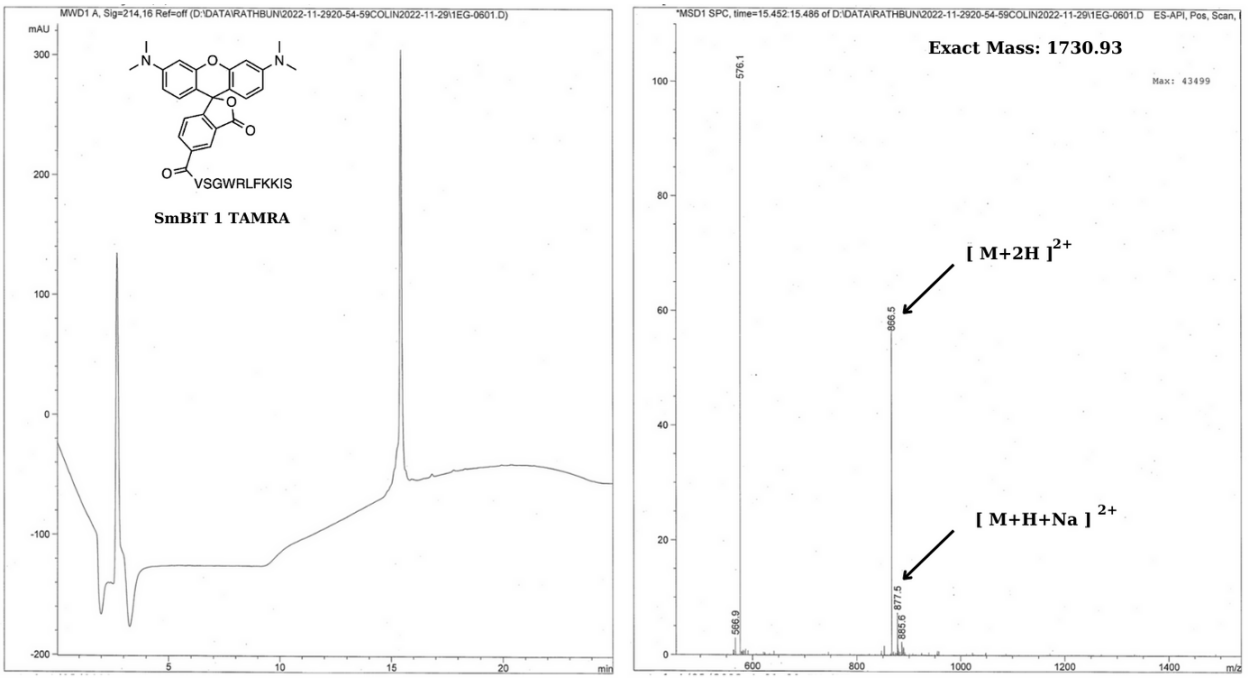

Figure S3: Characterization of SmBiT 1 - TAMRA

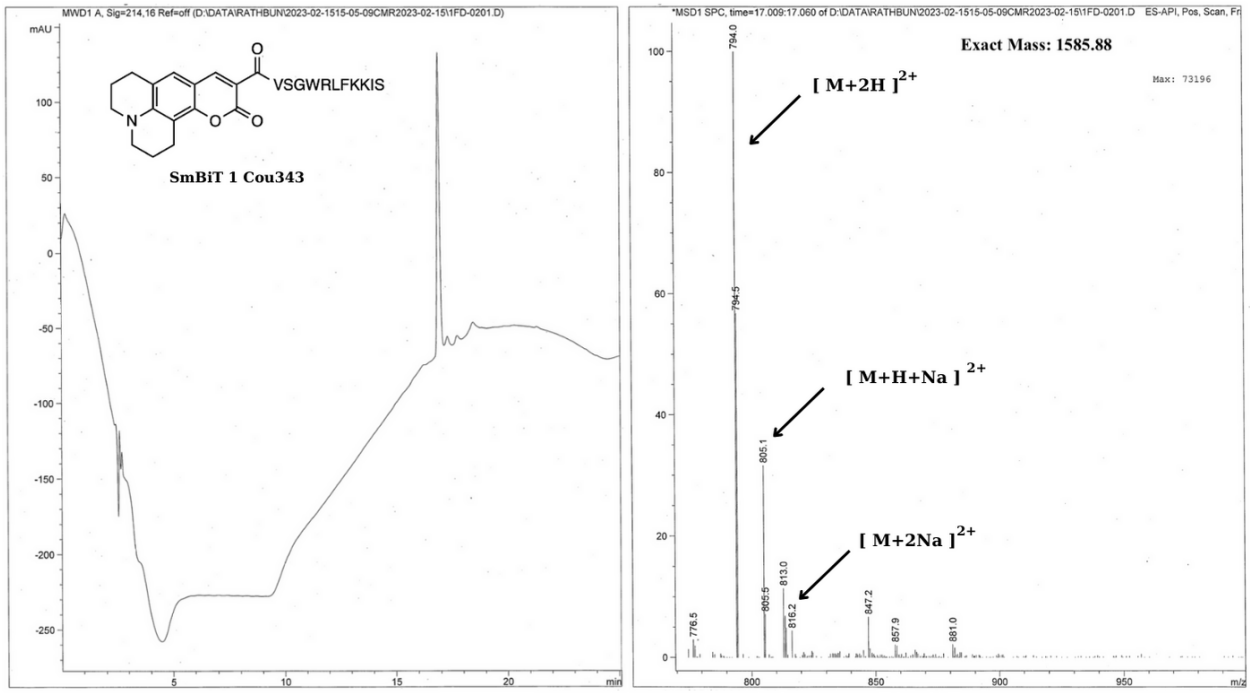

Figure S4: Characterization of SmBiT 1 - Cou343

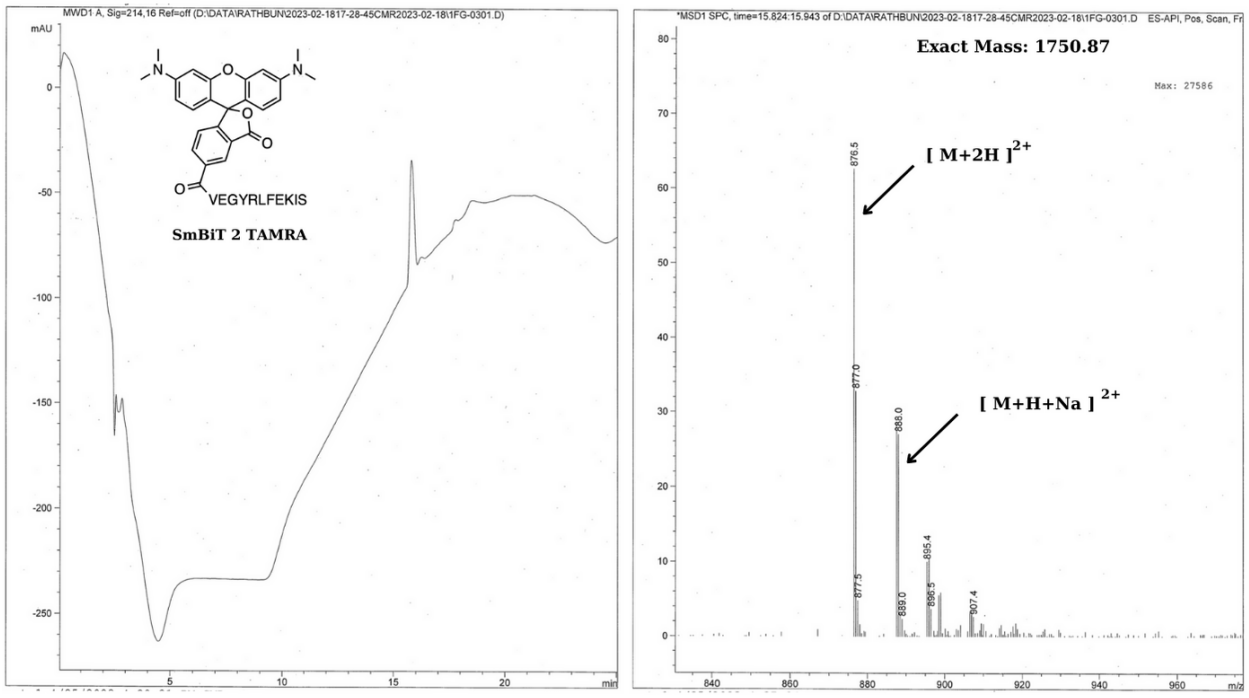

Figure S5: Characterization of SmBiT 2 - TAMRA

References

(1) Paley, M. A.; Prescher, J. A. Bioluminescence: a versatile technique for imaging cellular and molecular features. *MedChemComm* **2014**, *5*, 255–267.

(2) Roda, A., *Chemiluminescence and bioluminescence: past, present and future*; Royal Society of Chemistry: 2011.

(3) Choy, G.; O'Connor, S.; Diehn, F. E.; Costouros, N.; Alexander, H. R.; Choyke, P.; Libutti, S. K. Comparison of noninvasive fluorescent and bioluminescent small animal optical imaging. *Biotechniques* **2003**, *35*, 1022–1030.

(4) Lewis, M. D.; Fortes Francisco, A.; Taylor, M. C.; Burrell-Saward, H.; McLatchie, A. P.; Miles, M. A.; Kelly, J. M. Bioluminescence imaging of chronic T rypanosoma cruzi infections reveals tissue-specific parasite dynamics and heart disease in the absence of locally persistent infection. *Cellular Microbiology* **2014**, *16*, 1285–1300.

(5) Song, G.; Wu, Q.-P.; Xu, T.; Liu, Y.-L.; Xu, Z.-G.; Zhang, S.-F.; Guo, Z.-Y. Quick preparation of nanoluciferase-based tracers for novel bioluminescent receptor-binding assays of protein hormones: using erythropoietin as a model. *Journal of Photochemistry and Photobiology B: Biology* **2015**, *153*, 311–316.

(6) Yasuzaki, Y.; Yamada, Y.; Ishikawa, T.; Harashima, H. Validation of mitochondrial gene delivery in liver and skeletal muscle via hydrodynamic injection using an artificial mitochondrial reporter DNA vector. *Molecular Pharmaceutics* **2015**, *12*, 4311–4320.

(7) Hall, M. P.; Unch, J.; Binkowski, B. F.; Valley, M. P.; Butler, B. L.; Wood, M. G.; Otto, P.; Zimmerman, K.; Vidugiris, G.; Machleidt, T., et al. Engineered luciferase reporter from a deep sea shrimp utilizing a novel imidazopyrazinone substrate. *ACS Chemical Biology* **2012**, *7*, 1848–1857.

(8) Dixon, A. S.; Schwinn, M. K.; Hall, M. P.; Zimmerman, K.; Otto, P.; Lubben, T. H.; Butler, B. L.; Binkowski, B. F.; Machleidt, T.; Kirkland, T. A., et al. NanoLuc complementation reporter optimized for accurate measurement of protein interactions in cells. *ACS Chemical Biology* **2016**, *11*, 400–408.

(9) Zhao, H.; Doyle, T. C.; Coquoz, O.; Kalish, F.; Rice, B. W.; Contag, C. H. Emission spectra of bioluminescent reporters and interaction with mammalian tissue determine the sensitivity of detection in vivo. *Journal of Biomedical Optics* **2005**, *10*, 41210–41210.

(10) Wang, J.; Liu, G.; Cham-Fai Leung, K.; Loffroy, R.; Lu, P.-X.; Wang, X. J., et al. Opportunities and challenges of fluorescent carbon dots in translational optical imaging. *Current Pharmaceutical Design* **2015**, *21*, 5401–5416.

(11) Dale, N. C.; Johnstone, E. K.; White, C. W.; Pfleger, K. D. NanoBRET: the bright future of proximity-based assays. *Frontiers in Bioengineering and Biotechnology* **2019**, *7*, 56.

(12) Suzuki, K.; Kimura, T.; Shinoda, H.; Bai, G.; Daniels, M. J.; Arai, Y.; Nakano, M.; Nagai, T. Five colour variants of bright luminescent protein for real-time multicolour bioimaging. *Nature Communications* **2016**, *7*, 13718.

(13) Hiblot, J.; Yu, Q.; Sabbadini, M. D.; Reymond, L.; Xue, L.; Schena, A.; Sallin, O.; Hill, N.; Griss, R.; Johnsson, K. Luciferases with tunable emission wavelengths. *Angewandte Chemie* **2017**, *129*, 14748–14752.

(14) Fowler, D. M.; Fields, S. Deep mutational scanning: a new style of protein science. *Nature Methods* **2014**, *11*, 801–807.

(15) McGahan, A. F.; Rathbun, C. Identifying mutations of NanoBiT to increase selectivity for multicomponent cellular tracking. *Dickinson BCMB Thesis* **2022**.

(16) Unger, E. K.; Keller, J. P.; Altermatt, M.; Liang, R.; Matsui, A.; Dong, C.; Hon, O. J.; Yao, Z.; Sun, J.; Banala, S., et al. Directed evolution of a selective and sensitive serotonin sensor via machine learning. *Cell* **2020**, *183*, 1986–2002.

(17) Melnikov, A.; Rogov, P.; Wang, L.; Gnirke, A.; Mikkelsen, T. S. Comprehensive mutational scanning of a kinase in vivo reveals substrate-dependent fitness landscapes. *Nucleic Acids Research* **2014**, *42*, e112–e112.

(18) Fernández-Carneado, J.; Giralt, E. An efficient method for the solid-phase synthesis of fluorescently labelled peptides. *Tetrahedron Letters* **2004**, *45*, 6079–6081.

(19) Brennan, C. K.; Ornelas, M. Y.; Yao, Z. W.; Prescher, J. A. Multicomponent bioluminescence imaging with naphthylamino luciferins. *ChemBioChem* **2021**, *22*, 2650–2654.